Layout optimization of heaving Wave Energy Converters linear arrays in front of a vertical wall

Loukogeorgaki, Eva; Michailides, Constantine ; Lavidas, G.; Chatjigeorgiou, Ioannis K.

DOI
10.1016/j.renene.2021.07.040

Publication date
2021

Document Version
Final published version

Published in
Renewable Energy

Citation (APA)
Loukogeorgaki, E., Michailides, C., Lavidas, G., & Chatjigeorgiou, I. K. (2021). Layout optimization of heaving Wave Energy Converters linear arrays in front of a vertical wall. *Renewable Energy*, *179*, 189-203. https://doi.org/10.1016/j.renene.2021.07.040

Renewable Energy 179 (2021) 189–203

Contents lists available at ScienceDirect

Renewable Energy

journal homepage: www.elsevier.com/locate/renene

Layout optimization of heaving Wave Energy Converters linear arrays in front of a vertical wall

Eva Loukogeorgaki [a, *], Constantine Michailides [b], George Lavidas [c], Ioannis K. Chatjigeorgiou [d]

[a] Department of Civil Engineering, Aristotle University of Thessaloniki, Thessaloniki, 54124, Greece
[b] Department of Civil Engineering and Geomatics, Cyprus University of Technology, Limassol, 3036, Cyprus
[c] Faculty of Civil Engineering and Geosciences, Department of Hydraulic Engineering, Delft University of Technology, Delft, 2628, CN, the Netherlands
[d] School of Naval Architecture and Marine Engineering, National Technical University of Athens, Athens, 15780, Greece

ARTICLE INFO

Article history:
Received 16 March 2021
Received in revised form
29 May 2021
Accepted 8 July 2021
Available online 9 July 2021

Keywords:
Wave energy converters
Array
Vertical wall
Optimization
Genetic algorithms
Greece

ABSTRACT

The present paper focuses on the determination of optimum layouts for linear arrays of heaving Wave Energy Converters (WECs) in front of a vertical wall. Optimum layouts maximize the annual averaged absorbed energy at a given marine site and satisfy spatial constraints. For achieving this goal, we developed an efficient optimization numerical framework, where a genetic algorithm solver is appropriately coupled with a frequency-domain hydrodynamic model, while, furthermore, a numerical wave model is utilized to determine the local wave climate conditions at the site of interest. The context is applied for an array of five semi-immersed, oblate spheroidal heaving WECs deployed at five near-shore sites of mild wave environments in the Aegean Sea, Greece. For each site, different optimization cases are solved, facilitating the investigation of different aspects of the examined problem. The largest annual energy absorption ability is observed for optimum layouts, characterized by the placement of the array close to the wall and the formation of clusters of closely-positioned WECs near the wall edges. Compared to arrays employed at sites in south-eastern Aegean, optimally-arranged arrays at central Aegean locations showed reduced energy absorption ability due to milder local wave conditions and/or the existence of quite limited water depths.

1. Introduction

Wave energy presents an abundant, clean source of offshore renewable energy that can contribute to the satisfaction of the European Union's energy and climate targets towards electricity generation decarbonization and climate change mitigation. This potential contribution has been also unveiled in the recent EU's Offshore Energy Strategy [1], where the target of 1 GW power extraction from different ocean energy technologies by 2030 was set. The significance of the wave energy utilization has led to a rapid growth of the wave energy technology during the last decades, including the development and testing of various types of Wave Energy Converters (WECs) (e.g., Refs. [2,3]). Among these types, the heaving WECs (point absorbers) correspond, nowadays, to one of the two most advanced and technologically mature device types [4].

Irrespectively of the WEC type considered, the realization of large-scale commercial competitive solutions requires the deployment of multiple WECs arranged in arrays (e.g., Refs. [5–7]). The overall performance of these multi-body arrangements depends strongly upon the array's layout, as well as upon the characteristics (water depth and long-term wave resource) of the offshore or near-shore deployment site, similarly to single-unit WECs (e.g., Ref. [8]). At near-shore locations, lengthy coastal structures, ensuring the continuous and safe implementation of port-related operations and/or other coastal activities, may exist, while the relevant authorities and operators may seek for alternative combined uses of these facilities in order to attain sustainability and reduce their carbon footprint. Along these lines, arrays of heaving WECs could be deployed in front of vertical (wall-type) breakwaters, enabling the exploitation of both the incident and the scattered from the

* Corresponding author.
E-mail addresses: eloukog@civil.auth.gr (E. Loukogeorgaki), c.michailides@cut.ac.cy (C. Michailides), g.lavidas@tudelft.nl (G. Lavidas), chatzi@naval.ntua.gr (I.K. Chatjigeorgiou).

https://doi.org/10.1016/j.renene.2021.07.040
0960-1481/

leeward boundary waves. This approach falls also within the wider framework of integrating WECs with various types of coastal structures (e.g., Refs. [9–14]) and, thus, it has many advantages, such as efficient use of the marine space, realization of cost-efficient solutions through costs sharing and boost of the WECs' maturity.

The performance of various linear arrays of heaving WECs in front of a vertical, bottom-mounted wall has been investigated and assessed in the frequency domain by various researchers. More specifically, Mavrakos et al. [15] assessed the power absorption ability of an array of five cylindrical WECs, while assuming a leeward boundary of infinite length. Under the same assumption, the performance of a linear, parallel, or perpendicular to the wall, array of five vertical axisymmetric (cylindrical or conical or semi-spherical) heaving WECs was investigated in Refs. [16,17]. The existence of a finite length leeward wall was considered in Refs. [18,19]. Those studies assessed the hydrodynamic behavior and the power absorption ability of a linear array of nine cylindrical and five oblate spheroidal, respectively, heaving WECs. In all the above investigations, specific array layouts were taken into account, characterized by equally-spaced WECs situated at predefined, fixed, locations with respect to the wall. Most of these investigations, however, illustrated the direct dependence of the array's power absorption ability upon the locations of the WECs with respect to the wall and within the array. Accordingly, the determination of optimum array layouts can be considered essential towards the efficient deployment of heaving WECs in front of wall-type coastal structures. This, in turn, requires the development and application of integrated optimization processes, where optimum solutions are sought by taking into account the hydrodynamics of the multi-body arrangement in the presence of the wall, as well as the local wave climate of the deployment site.

Up to now, various optimization methods and relevant processes have been developed and utilized by various researchers for the case of isolated (i.e., without the presence of the wall) arrays [20]. Child and Venupogal [21] studied the effect of the spatial configuration of WECs arrays in terms of the total absorbed power by coupling an analytical hydrodynamic model with two different optimization methods; the parabolic intersection method and the Genetic Algorithms (GAs). They concluded that superior results may be obtained using the GAs, although considerably more computational effort is required. Optimum layouts for arrays of five WECs were determined in Ref. [22], by developing a genetic algorithm approach that utilizes an analytical hydrodynamic model and integrates an array cost model. Ruiz et al. [23] compared three different optimization algorithms for WECs arrays problems, namely, the covariance matrix adaptation evolution strategy, the GAs and the glowworm swarm optimization algorithm. The results showed a slightly better performance for the two latter algorithms; however, the first algorithm turned out to be significantly less demanding relative to the computation effort required. Apart from the traditional evolutionary optimization algorithms, optimum layouts for isolated arrays have been determined by developing and deploying advanced approaches, such as the machine learning approach [24] and the artificial neural networks [25].

In the present paper, we present an efficient Optimization Numerical Framework (ONF) to determine the optimum layout of a linear array of heaving WECs in front of a vertical, bottom-mounted wall of finite length. The term “optimum” corresponds to layouts that maximize the annual averaged energy absorbed by the array at a marine site of interest, while, simultaneously, satisfying specific spatial constraints. The developed ONF consists of a GAs optimization solver, appropriately coupled with a frequency-domain hydrodynamic model, which solves the diffraction/radiation problem of the multi-body arrangement in the presence of the wall, and of a numerical wave model that determines the wave climate matrix of the deployment site. The framework is applied for an array of five identical, semi-immersed, oblate spheroidal heaving WECs deployed at five near-shore sites of mild wave environments in the Aegean Sea, Greece. For each site, three different optimization cases are assumed and solved, focusing on the determination of the optimum array-wall distance and the effect of the available, for placing the array, wall length on the optimum layouts and the absorbed energy. Emphasis is also given to the effect of the local wave climate and the water depth conditions on the maximized annual absorbed energy.

The remainder of the paper is organized as follows: In Section 2, the examined constrained optimization problem is numerically formulated, while Section 3 presents the proposed ONF and provides a detailed description of its components. In Section 4, the characteristics of the examined cases are cited, whereas Section 5 includes the results of the present investigation. Finally, in Section 6, conclusions are drawn, and an outlook for future applications is presented.

2. Problem's formulation

A linear array of Q hydrodynamically interacting, semi-immersed heaving WECs is placed in front of vertical, bottom-mounted wall of finite length l_w and of negligible thickness at a marine site of finite and constant water depth h (see Fig. 1). The array consists of identical WECs, which have an oblate spheroidal shape of equatorial radius (semi-major axis) a and polar radius (semi-minor axis) b (Fig. 1b). Each WECq, $q = 1, \ldots, Q$, is assumed to absorb power through a linear PTO mechanism, which is schematically represented in Fig. 1b as a linear damping system of damping coefficient b_{PTOq}, $q = 1, \ldots, Q$. All the WECs of the array are placed at a perpendicular distance c from the wall and they are distributed randomly along the length of the leeward boundary (Fig. 1a). The marine site, where the array and the wall are situated, is characterized by its local wave climate (i.e., set of sea states), where each sea state (long-crested irregular waves) is described by a wave spectrum of significant wave height H_s and peak period T_p and has an annual probability of occurrence $Pr(H_s, T_p)$.

Let the X, Y coordinates of the centers of the WECs in the global $OXYZ$ coordinate system (Fig. 1a), X_q and $Y_q \equiv c$, $q = 1, \ldots, Q$, respectively, denote the unknown locations of the devices in front of the wall. We seek to determine the optimum values of X_q, $q = 1, \ldots, Q$, and c, or, equivalently, the optimum layout of the WECs in front of the wall, so that the annual averaged energy absorbed by the whole array, E_{annual}, at the examined marine site is maximized, while, specific spatial constraints are satisfied. By defining X_q, $q = 1, \ldots, Q$, and c, as the design variables and E_{annual} as the objective function to be maximized, the constrained optimization problem considered herein, is expressed mathematically as:

$$\text{maxmize } E_{annual}(c, X_1, \ldots, X_q, \ldots, X_Q) \tag{1}$$

subjected to the following spatial constraints:

$$X_q - X_{q-1} \geq 2a, q = 2, \ldots, Q \tag{2}$$

$$\begin{cases} X_1 = l_{out} \\ X_Q = l_w - l_{out} \end{cases} \tag{3a}$$

or

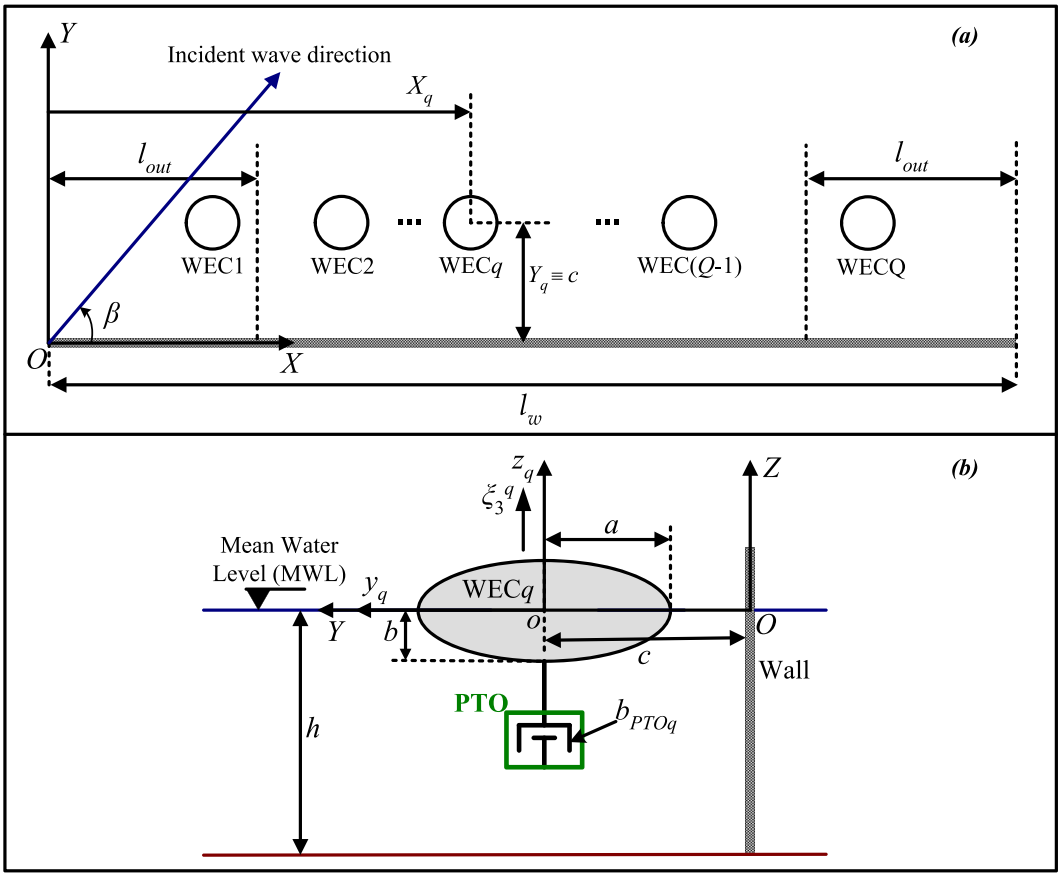

Fig. 1. Geometry of the examined arrangement and definition of basic quantities: (a) X–Y plane; (b) $Y-Z$ plane.

$$\begin{cases} 0 \le X_1 \le l_{out} \\ 0 \le l_w - X_Q \le l_{out} \end{cases} \tag{3b}$$

$$X_q \in [0, l_w], q = 1, \ldots, Q \tag{4}$$

$$1.1a \le c \le 4a \tag{5}$$

Eq. (2) expresses mathematically the avoidance of overlapping between two adjacent devices, while Eqs. (3a) and (3b) impose restrictions on the location of the two outer WECs along the wall, so that different aspects of the examined physical problem can be tackled. More specifically, by denoting with l_{out} the parts of l_w close to the wall edges, where only the two outer WECs of the array can be deployed (Fig. 1a), the application of Eq. (3a) expresses physically the utilization of a part of the total available wall length l_w for placing the WECs of the array. Alternatively, by applying Eq. (3b), the two outer WECs are allowed to be situated within l_{out} (i.e., along a length close to the wall edges), facilitating the formation of optimum array layouts within the total available wall length l_w. Continuing with the rest spatial constraints, Eq. (4) ensures the placement of all the WECs in front of the wall boundary, and, finally, Eq. (5) impose spatial restrictions on the perpendicular distance of the linear array from the wall. Specifically, the lower bound of Eq. (5) expresses mathematically the avoidance of overlapping between the WECs and the wall, while the upper bound of this equation ensures that the WECs are not situated far from the wall boundary. The value of the upper bound has been selected by considering also the parametric results of Loukogeorgaki et al. [19], who illustrated that the placement of a linear array of oblate spheroidal WECs at $c > 3a$ reduces the array's power absorption ability.

3. Numerical modelling and solution

In order to solve the constrained optimization problem of Section 2 for a given marine site characterized by a specific wave climate, a suitable ONF consisting of three numerical components (Fig. 2) is developed and applied. The first component corresponds to a frequency-domain Hydrodynamic Model (HyM) that solves the diffraction/radiation problem of the examined multi-body arrangement in the presence of the wall. Accordingly, it enables the calculation of the power absorbed by the WECs of the array for unit-amplitude monochromatic waves and, then, by performing a spectral analysis it facilitates the computation of the annual averaged energy absorbed by the array for the wave climate of the examined site. The second component corresponds to a GAs optimization Solver (GAS), which is appropriately coupled in an integrated computational environment with the HyM and solves the optimization problem. Finally, for estimating the required characteristics of the sea states (H_s, T_p and $Pr(H_s, T_p)$) and, thus, determining the required wave climate matrix of the marine site of interest, a Numerical Wave Model (NWM) is utilized, representing the third component of the proposed ONF. In the following sections, the three numerical components of the developed ONF as well as the coupling procedure of the HyM with the GAS are described in detail.

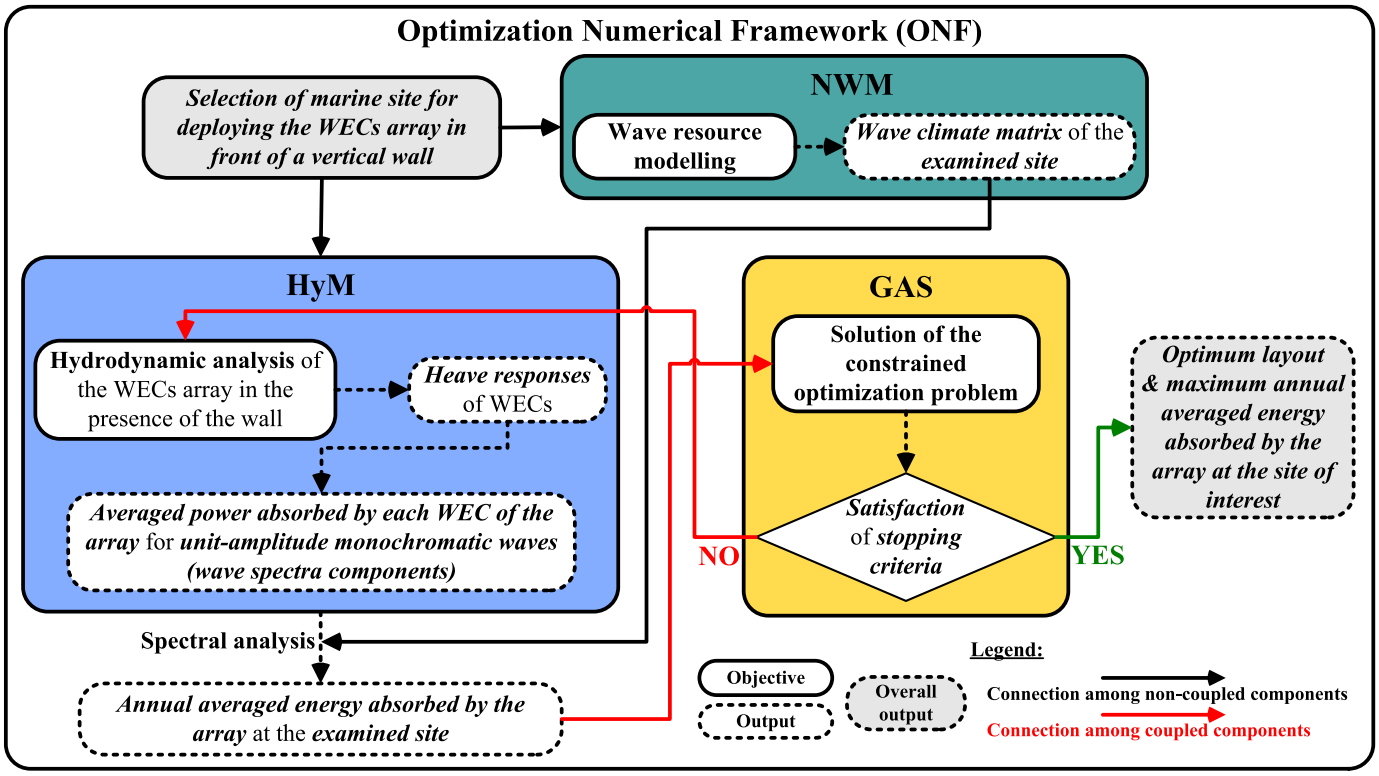

Fig. 2. Outline and components of the developed ONF.

3.1. Hydrodynamic model

The hydrodynamic analysis of the WECs array in front of the vertical wall under the action of monochromatic incident waves, taking into account the hydrodynamic interactions among the WECs and between the wall and the WECs, is conducted in the frequency domain and it relies on the Boundary Integral Equation Method (BIEM), which is numerically realized using the WAMIT code [26]. The relevant analysis is based on a three-dimensional linear potential theory, where, the wall is taken fixed at its position, while all devices are assumed to undergo small amplitude oscillations only along their working direction, i.e., along the local vertical oz_q axis (Fig. 1b). Hence, for all WECs, all degrees of freedom, except the one corresponding to heave, are considered ideally restricted. Assuming inviscid and incompressible fluid with irrotational flow, the fluid's motion is described by introducing the velocity potential. Its complex spatial part is defined as follows [26,27]:

$$\varphi = \underbrace{\varphi_I + \varphi_S}_{\varphi_D} + i\omega \sum_{q=1}^{Q} \xi_3^q \varphi_q \tag{6}$$

$$\varphi_I = \frac{igA}{\omega} \frac{\cosh[k(Z+h)]}{\cosh(kh)} e^{-ik(X\cos\beta + Y\sin\beta)} \tag{7}$$

where φ_I is the velocity potential of the incident waves, φ_S is the scattered potential, associated with the scattered disturbances of the incident waves from the WECs and the wall, φ_D denotes the diffraction potential, φ_q, $q = 1, \ldots, Q$, are the radiation potentials, associated with the waves radiated from the WECs due to their forced motion in heave and ξ_3^q correspond to the complex amplitudes of the WECs' heave motions. Furthermore, ω and A are the frequency and the amplitude, respectively, of the incident waves, that propagate at angle β relative to the global OX axis (Fig. 1a), g is the gravitational acceleration, k is the wave number and $i^2 = -1$.

The velocity potentials φ_m ($m = D$ or $m = q$) satisfy the Laplace equation in the entire fluid domain, while, furthermore, they are subjected to the following linearized boundary conditions corresponding to the combined kinematic and dynamic free-surface condition (Eq. (8)), the bottom boundary condition (Eq. (9)), and the Neumann boundary conditions on the wetted surface of the bodies (Eq. (10) and (11)).

$$\frac{\partial \varphi_m}{\partial Z} = \frac{\omega^2}{g} \varphi_m \; on \; Z = 0 \tag{8}$$

$$\frac{\partial \varphi_m}{\partial Z} = 0 \; on \; Z = -h \tag{9}$$

$$\frac{\partial \varphi_D}{\partial n} = 0 \tag{10}$$

$$\frac{\partial \varphi_q}{\partial n} = n_3^q \; for \; q = 1, \ldots, Q \tag{11}$$

In Eq. (11), n_3^q corresponds to the normal unit vector of WECq in the vertical direction.

Green's theorem is employed in order to cope with the boundary value problem of the unknown diffraction and radiation potentials of all bodies (WECs and wall) and of the WECs respectively. The solution of the problem relies on a three dimensional low-order panel method [26,27], where dipole panels [27] are assumed to model the wetted surface of the wall, given that the thickness of the bottom-mounted boundary is considered to be negligible.

Having solved the aforementioned boundary value problem, the first-order hydrodynamic forcing quantities and hydrodynamic parameters are calculated as follows:

$$F_3^q = -i\omega\rho\iint_{S_W^q} n_3^q \varphi_D ds, q = 1, ..., Q \tag{12}$$

$$A_{ql} - \frac{i}{\omega}B_{ql} = \rho\iint_{S_W^q} n_3^q \varphi_l ds, q, l = 1, ..., Q \tag{13}$$

where F_3^q is the heave exciting force applied on the qth WEC, A_{ql} and B_{ql} are the added mass and radiation damping coefficients respectively, S_W^q is the wetted surface of the qth WEC and ρ is the water density.

The complex amplitudes of the WECs' heave motions, ξ_3^q, $q = 1$, …, Q, are, then, obtained by solving the following linear system of equations:

$$\sum_{q=1}^{Q}\left[-\omega^2\left(M_{ql}+A_{ql}\right)+i\omega\left(B_{ql}+B_{ql}^{PTO}\right)+C_{ql}\right]\xi_3{}^q = F_3{}^l, l = 1, ..., Q \tag{14}$$

In Eq. (14), M_{ql} and C_{ql} are, respectively, the mass matrix and the hydrostatic-gravitational stiffness coefficients, while B_{ql}^{PTO} correspond to the damping coefficients originating from the PTO mechanism. For a qth WEC, the latter mechanism is modeled as a linear damping system (Fig. 1b), with constant damping coefficient b_{PTOq}, actuated from the heave motion of the WEC. Accordingly, in Eq. (14), $B_{ql}^{PTO} = b_{PTOq}$ for $q = l = 1$, …, Q, whereas $B_{ql}^{PTO} = 0$ for $q \neq l$.

Under the action of monochromatic unit-amplitude incident waves of frequency ω, the averaged power, $p_q(\omega)$, absorbed by the qth WEC of the array follows from:

$$p_q(\omega) = \frac{1}{2}b_{PTOq}\omega^2\left|\xi_3^q\right|^2 \tag{15}$$

where $\left|\xi_q^3\right|$ is the amplitude of the complex quantity ξ_3^q.

Subsequently to the calculation of $p_q(\omega)$ for various ω values representing the frequency components of a spectrum, a spectral analysis is performed in order to estimate the annual averaged energy absorbed by the array for the wave climate conditions of the examined marine site. Initially, for each sea state described by a spectrum of H_s and T_p, the averaged power absorbed by the linear array, $p(H_s, T_p)$, is obtained as follows:

$$p(H_s,T_p) = \sum_{q=1}^{Q} p_q(H_s,T_p) = \sum_{q=1}^{Q}\int_0^{\infty} S_{TMA}(\omega|H_s,T_p)p_q\left(\omega\right)d\omega \tag{16}$$

where $p_q(H_s,T_p)$, $q = 1$, …, Q, is the averaged power absorbed by the qth device for the given sea state, $S_{TMA}(\omega|H_s,T_p)$ is the spectral density of the TMA spectrum [28–31], while the symbol "|" is used to denote given values of H_s and T_p. The integral part of Eq. (16) implies summation of the averaged power absorbed by a qth WEC over the frequency components of the discretised spectrum.

The TMA spectrum is deployed in the present paper in order to consider through a robust and simple method, limited water depth conditions, as exist at near-shore locations, where the proposed arrangement (WECs and wall) can be realized. More specifically, the TMA spectrum has a finite depth spectral formulation and corresponds to a modified JONSWAP spectrum in shallow waters. For a given sea state of H_s and T_p, $S_{TMA}(\omega|H_s,T_p)$ can be obtained by multiplying the corresponding spectral density of the JONSWAP spectrum, $S_{JONSWAP}(\omega|H_s,T_p)$, with the so-called "limited depth" function, $\Phi(h,\omega)$, that depends upon the depth h and the frequency, ω (e.g., Refs. [30,31]). Hence,

$$S_{TMA}(\omega|H_s,T_p) = S_{JONSWAP}(\omega|H_s,T_p)\Phi(h,\omega) \tag{17}$$

The function $\Phi(h,\omega)$ is given by (e.g., Ref. [31]):

$$\Phi(h,\omega) = \begin{cases} 0.5\left(\omega\sqrt{h/g}\right)^2 & \text{for } \omega\sqrt{h/g} < 1 \\ 1.0 - 0.5\left(2-\omega\sqrt{h/g}\right)^2 & \text{for } 1 \le \omega\sqrt{h/g} < 2 \\ 1.0 & \text{for } \omega\sqrt{h/g} \ge 2 \end{cases} \tag{18}$$

The spectral density of the JONSWAP spectrum $S_{JONSWAP}(\omega|H_s, T_p)$, is obtained by applying Eq. (19) [32]:

$$S_{JONSWAP}(\omega|H_s,T_p) = (1-0.287\ln(\gamma))\frac{5}{16}H_s^2\omega_p^4\omega^{-5}\exp\left(-\frac{5}{4}\left(\frac{\omega}{\omega_p}\right)^{-4}\right)\gamma^{\exp\left(-0.5\left(\frac{\omega-\omega_p}{\sigma\omega_p}\right)^2\right)} \tag{19}$$

where $\omega_p = 2\pi/T_p$, γ is the non-dimensional peak shape parameter equal to 3.3 and σ is the spectral width parameter equal to 0.07 for $\omega \le \omega_p$ and 0.09 for $\omega > \omega_p$.

Given the annual probability of occurrence of each sea state, $Pr(H_s,T_p)$, at the marine site, where the multi-body arrangement is deployed, the annual averaged energy absorbed by the whole array, E_{annual}, is, finally, calculated as:

$$E_{annual} = 8,760\left(\sum_{H_s}\sum_{T_p} Pr(H_s,T_p)p(H_s,T_p)\right) \tag{20}$$

Eq. (20) expresses mathematically the objective function of the constrained optimization problem defined in Section 2.

3.2. GAs optimization solver and its coupling with the hydrodynamic model

The utilized in the present paper GAS corresponds to meta-heuristic optimization algorithm that relies on an intelligent search within the finite solution space by mimicking the process of biological evolution; namely, a population of individuals (i.e., candidate solutions of the optimization problem) is evolving in time according to the "survival of the fittest" rule, implying that the fittest (superior) individuals can be considered for reproduction in the generation of the next population. The population successively approaches an optimum solution, since "good" parents generate

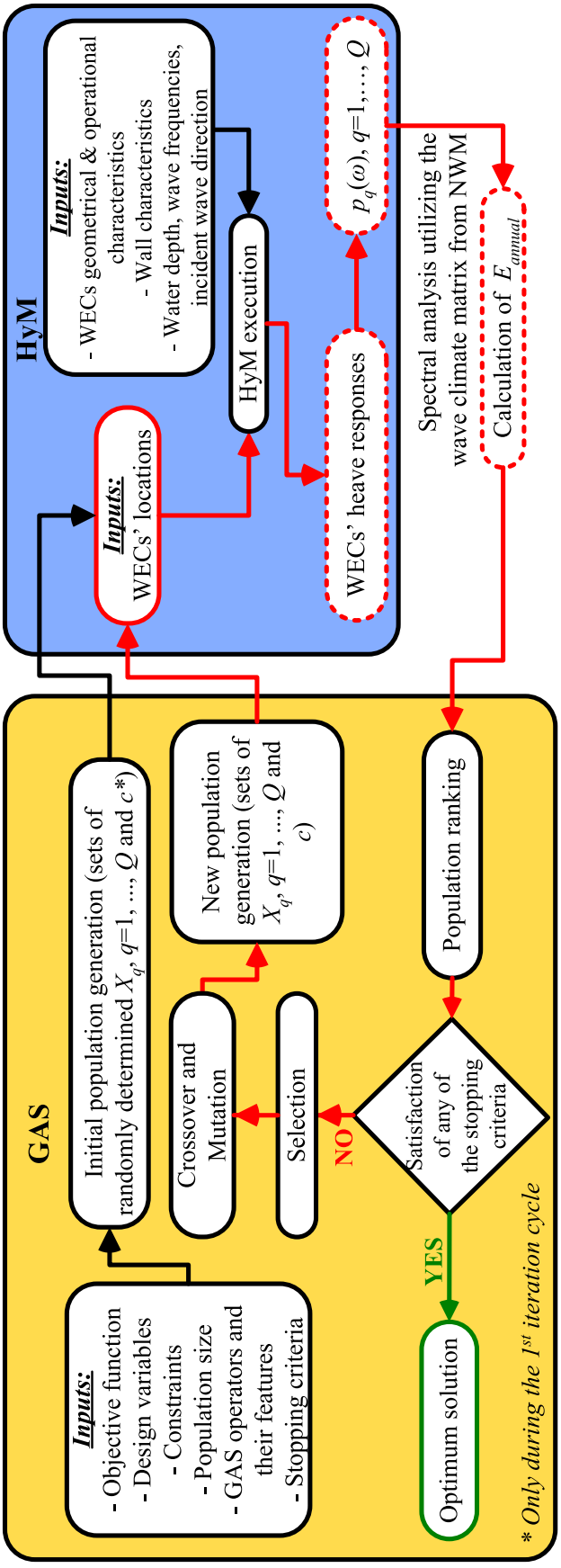

Fig. 3. GAS process for finding the optimum solution including the GAS-HyM coupling.

"good" children. Within this context, a randomized, but well-structured optimization process is realized within the GAS, as shown in Fig. 3, where also details about the coupling of the GAS with the HyM are provided.

Initially, the design variables X_q, $q = 1, \ldots, Q$ and c, the objective function $E_{annual}(c, X_1, \ldots, X_q, \ldots, X_Q)$ (Eq. (20)), the constraints (Eqs. (2)–(5)) and the size of the population (equal to the number of individuals) are given as input in the GAS. Moreover, the features of the GAS operators selected for generating the individuals for each successive population (i.e., ranking, selection, mutation and crossover) are determined and the stopping criteria of the optimization algorithm are defined. During the GAS execution, each individual of a population corresponds to a set of values of X_q, $q = 1, \ldots, Q$ and c, and, thus, to a candidate solution of the optimization problem, while the size of the population remains constant.

The optimization process starts by creating a constraint dependent random initial population for the design variables based on a uniform random sampling over lower and upper bound values (Eqs. (4) and (5)) and the rest spatial constraints (Eqs. (2) and (3)). Each individual of the initial population is used as input to the HyM together with the values of the rest physical quantities required in the latter numerical model. HyM is executed, the heave responses of the WECs are obtained and the power absorbed by the WECs for unit-amplitude waves (Eq. (15)) is calculated. The objective function, E_{annual} (Eq. (20)), is, then, quantified for the examined site by deploying, within the relevant spectral analysis, the corresponding wave climate matrix (H_s, T_p and $Pr(H_s, T_p)$) as obtained from the NWM. Based on the calculated E_{annual} values, ranking of the initial population in descending order follows, starting from the individual that has the best score (i.e., the highest E_{annual} value), and the stopping criteria of the optimization algorithm are checked. These criteria are related with: (a) a predefined maximum number of iterations and (b) an average change of the objective function value over a number of iterations compared to a predefined tolerance value. If any of these criteria is not satisfied, a new population of individuals is generated by deploying specific GAS operators, while imposing constraints and bounds for the design variables (Eqs. (2)–(5)). The selection operator is, initially, utilized, where an upper percentage of individuals in the ranked population is selected to survive and continue to the next generation. Among these individuals, those having the highest ranking are selected as "elite" and are maintained within the next population without any change, while, the rest are selected as "parents". The "parents" are, then, used to generate new individuals by: (a) combining the entries of a pair of "parents" to create fitter offspring (crossover operator of GAS) and (b) changing randomly a single "parent", so that diversity within the population is maintained (mutation operator of GAS). The above operators ensure that all solution space regions will be explored, while preventing the algorithm to stuck in local minima. The individuals of the new population are used as input to the HyM for implementing hydrodynamic analysis and, thus, calculating new values of E_{annual} (Eq. (20)), by deploying once more the wave climate matrix (H_s, T_p and $Pr(H_s, T_p)$) of the examined site. The individuals of the new population are ranked, and the stopping criteria are again checked. The iterative process continues until one of the stopping criteria is satisfied. When this is achieved, the individual of the last generated population having the best ranking is assigned as the optimum solution of the examined constrained maximization problem. In the present paper, GAS is numerically realized by using the Optimization Toolbox™ R2019b [33] of MATLAB [34]. GAS is coupled with the HyM within the same computational environment.

3.3. Wave numerical model

Wave climate information is not universal and differs around regions, depending on local bathymetric and climatic conditions. Therefore, to properly tackle problems related to WECs' development and deployment, long-term accurate realistic wave parameter data are necessary. Within this context, this study utilizes the Simulating WAves Nearshore (SWAN), a spectral phased averaged model that estimates the wave variance spectrum through space (latitude, longitude) and time. SWAN incorporates this iterative solution using different source terms (see Eq. (21)) that allow for multiple physical elements to be implemented and interact, to obtain the wave spectra.

$$S_{tot} = S_{in} + S_{nl3} + S_{nl4} + +S_{ds,w} + S_{ds,b} + S_{ds,br} \quad (21)$$

In Eq. (21), S_{tot} is the total source term accounting for all physical processes that generate, dissipate, or redistribute energy, S_{in} is the input of energy represented by wind growth, S_{nl3} and S_{nl4} represent triad and quadruplet interactions, responsible for the re-distribution of frequencies in shallow and deep waters respectively, while S_{ds} are usually dissipation (negative) source terms that reduce the energy content and alter the wave characteristics. More specifically, $S_{ds,w}$ is for white-capping, $S_{ds,b}$ is for bottom friction (influenced by soil composition, etc) and $S_{ds,br}$ is for bottom breaking.

For applications at near-shore locations, SWAN can resolve implicitly complex triad interactions (S_{nl3}), bottom friction and breaking ($S_{ds,b}$, $S_{ds,br}$), and refraction effects [35–37]. While other oceanic model may use explicit solutions for near-shore conditions, this can often lead to over-estimation of wave parameters, as the frequency exchanges is "biased" to lower frequencies.

Another important factor that affects the quality of the wave generated data, are the wave growth physics dependencies upon the wind [38], hence, the significant impacts that wind drivers have on wave generation and quadruplet interactions [39–42]. Prior to any model consideration, the NWM chosen, including SWAN, must be calibrated and validated, clearly discussing the accuracy and limitations of the model, with consideration on its applicability [43].

4. Characteristics of examined cases

The ONF developed in this study is applied for five marine sites located in the Aegean Sea, Greece (Fig. 4). Sites S1~S3 correspond to near-shore locations at Siros, Anafi and Antiparos islands of the Cyclades island complex in the central Aegean, while sites S4~S5 correspond to similar locations at Kasos and Karpathos islands of Dodecanese situated in the south-eastern Aegean. The selection of these sites has been mainly based on the results of availability and accessibility analysis in the Mediterranean and Aegean Seas of [44,45]. This analysis illustrated the existence of better-than-expected capacity factors and high accessibility at these marine areas in the case of near-shore heaving devices' deployment. Other factors, such as the existence of a vertical breakwater (e.g., site S1) or the necessity to build a breakwater (e.g., site S2) were also taken into account.

For each of the above marine sites, optimum layout configurations are determined for a linear array of $Q = 5$ oblate spheroidal WECs (Fig. 1a with $Q = 5$) of equatorial radius $a = 2.0$ m and non-dimensional polar radius $b/a = 0.85$ placed in front of a wall of total non-dimensional length $l_w/a = 36$. The arrangement is oriented perpendicularly to the most predominant wave direction, which is assumed common for all sea states. The WECs' geometrical characteristics have been selected based on the previous works of [19,46]. All WECs within the array are taken to have the same PTO characteristics. Accordingly, in Eq. (14) $B_{ql}^{PTO} = b_{PTO}$ for $q = l = 1, \ldots, 5$. The constant damping coefficient, b_{PTO}, is appropriately tuned, in terms of maximizing energy absorption at the heave natural frequency, ω_{n3}^{iso}, of a single, isolated device. Hence, and in accordance with [47], b_{PTO} is considered to be equal with the heave radiation damping of a single, isolated WEC at $\omega = \omega_{n3}^{iso}$. For the examined WEC geometry, ω_{n3}^{iso} is 2.4 rad/s (the corresponding heave natural period, T_{n3}^{iso}, is 2.6 s), leading to $b_{PTO} = 10,322.20$ Ns/m [19]. HyM is

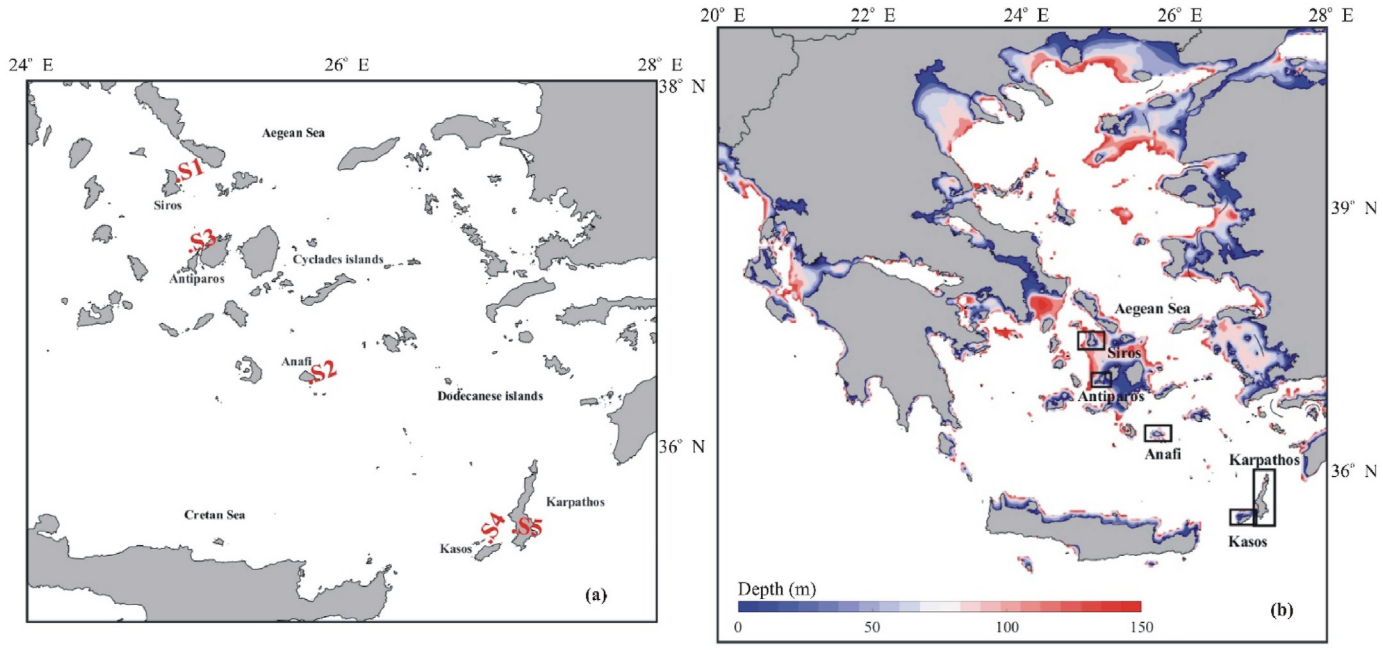

Fig. 4. Location of: **(a)** marine sites selected and **(b)** relevant Greek islands in the wider area of the Aegean Sea (depths shown are limited up to 150 m).

Table 1
Optimization cases investigated for each of the five marine sites in the Aegean Sea.

Optimization case	Non-dimensional design variables to be optimized	Non-dimensional values of rest design variables	l_{out}/a
OC1	c/a	$X_1/a = 10$, $X_2/a = 14$, $X_3/a = 18$, $X_4/a = 22$ and $X_5/a = 26$	10
OC2	X_q/a, $q = 2$, 3 and 4	Optimum c/a obtained from OC1, $X_1/a = 10$ and $X_5/a = 26$	10
OC3	X_q/a, $q = 1, \ldots, 5$	Optimum c/a obtained from OC1	10

applied for non-dimensional water depth h/a equal to 3.5, 4 and 5 for sites S1, S2 and S3~S5 respectively and for $\beta = 270^o$ (Fig. 1a), due to the perpendicular orientation of the arrangement relative to the most predominant wave direction, with frequency varying between 0.05 rad/s and 4.0 rad/s. The latter values correspond also to the cut-off spectral frequencies utilized in Eqs. (17)-(19) for performing the required spectral analysis.

Following a stepwise process, three optimization cases have been considered and successively solved for each of the S1~S5 sites (Table 1). OC1 corresponds to a simple constraint optimization problem of a single-variable, which seeks to determine the optimum non-dimensional perpendicular distance c/a of the linear array from the wall. The array is assumed to consist of equally-spaced WECs distributed at $10 \leq X/a \leq 26.0$ with a fixed center-to-center distance equal to $4a$. For solving OC1, only the spatial constraint described by Eq. (5) is taken into account. For the optimum c/a value obtained from OC1, OC2 aims at determining the optimum layout configurations of the array, by utilizing a part of the total available wall length equal to $16a$ for placing randomly the devices. In that respect, Eq. (3a) is applied with $l_{out} = 10a$ and the rest spatial restrictions are imposed by utilizing Eqs. (2) and (4). Finally, OC3 seeks to define optimum layout configurations of the array along the total available wall length. The array is again assumed to be situated at the optimum non-dimensional distance of the wall, c/a, as resulted from OC1. Accordingly, the optimization problem is solved taking into account the spatial constraints described by Eqs. (2), (3b) and (4). The application of Eq. (3b) allows the placement of the two outer WECs at any position within $l_{out} = 10a$. It is noted that the consideration of OC1~OC3, characterized by a different level of complexity, demonstrates the generic aspect of the proposed ONF and its ability to handle effectively different aspects of the examined physical problem.

Regarding the 2nd component of the proposed ONF, GAS is applied by defining the design variables, X_q, $q = 1, \ldots, 5$, and c, to have values up to their first decimal; thus, the WECs' optimum locations are determined within a 10 cm grid. Furthermore, aiming at keeping the computational effort at a reasonable level, while preserving the required numerical accuracy, the following options have been assigned to the optimization solver based on a relevant sensitivity analysis: (a) double vector population type with population size equal to 10, (b) adaptive feasible mutation, (c) 0.6 crossover fraction with constraint dependent crossover function, (d) guarantee of 2 individuals to survive in the next generation as elite count and (e) termination of the optimization process if the change in the objective function (E_{annual}) value over 8 iterations is less than 0.001 (critical stopping criterion). For each optimization case of Table 1, multiple different runs have been implemented, in order to ensure that the global maximum of the physical problem is correctly predicted by the GAS. Furthermore, a different number of GAS operator iterations was required for achieving convergence of the optimization algorithm. The minimum and maximum number of the required iterations among all examined cases was 9 and 17, respectively. Regarding the computational effort, by using a standard PC with 128 GB RAM and Intel® Xeon® Gold 6130 CPU@ 2.1 GHz 2.1 GHz (2 processors) the mean computational time for one iteration (10 runs of the HyM) was approximately equal to 140 min.

Finally, the sea states data for the five examined sites were obtained by a hindcast based on the SWAN model, developed specifically for the Aegean Sea [44]. The model used a two way nesting for the Mediterranean and the Aegean Seas and provided a comprehensive resource assessment of metocean conditions for 35 years from 1980 to 2014. The calibration included refined tuning of the wind growth and white capping elements for the Aegean Sea, with wind drivers obtained by the Climate Forecast System Reanalysis (CFSR) atmospheric dataset [48]. The Aegean Sea domain has a spatial resolution ≈2.0 km for latitude and longitude, while nearshore and shallow water terms were activated and tuned. Wave direction was discretised in 25 interval and wave frequencies in 30 bins distributed logarithmically, with the lowest set at 0.0357 Hz and the highest at 0.5 Hz. A "warm" start configuration was set in the model to minimize ramping up period in the wave model and minimize statistical under-estimations.

The hindcast database was also compared with other models run for the region, and it proved to provide the highest level of agreement amongst existing studies. Significant wave height biases were near zero with over-estimation of H_s from 0.01 cm to 0.1 cm, and a negligible under-estimation in T_p with −0.1 s. The detail model calibration/validation led to adopting this hindcast database, since in overall the database not only has the lowest mean annual biases, but due to its wind scheme parameterisation it has also the lowest extreme H_s biases, making it reliable to all seasons.

Based on the spatial resolution of the applied NWM, the 35-years H_s and T_p data for S1, S2 and S3 were obtained at a water depth equal to 11.5 m, 18.7 m and 19.0 m respectively, while the corresponding water depths for S4 and S5 were 19.2 m and 27.0 m respectively. In all sites, non-linear wave interactions, such as triad, refraction and shoaling have been considered in the application of SWAN.

5. Results and discussion

The wave climate matrices as obtained from the NWM for the five examined sites in the Aegean Sea are shown in Tables 2–6, where for each sea state the corresponding $Pr(H_s, T_p)$ value is expressed in terms of percentage (%).

All sites are characterized by a mild wave environment, since sea states of significant wave height up to 1.75 m (S1 and S3) or up to 2.25 m (S2, S4 and S5) show the largest probability of occurrence. For the sites located in the Cyclades (Tables 2–4), the most frequent sea states have $3.0\text{ s} \leq T_p \leq 6.0\text{ s}$ (S1 and S3) or $4.0\text{ s} \leq T_p \leq 6.0\text{ s}$ (S2). On the other hand, for S4 and S5 located in Dodecanese (Tables 5 and 6), sea states with large probability of occurrence are distributed within a wider T_p range, i.e., at $4.0\text{ s} \leq T_p \leq 8.0\text{ s}$.

Continuing with the optimization results, Fig. 5 shows schematically the optimum layout configurations of the array in front of the wall in the X–Y plane for sites S1~S5 and for OC1 (Table 1). For the examined linear array consisting of equally-spaced oblate spheroidal WECs with fixed positions along a part of the available wall length, optimum layout configurations for all sites are realized by placing the array at $c/a = 1.1$; namely, at the smallest allowable non-dimensional distance from the wall boundary. This outcome is

Table 2
Wave climate matrix for site S1 based on 35-years hindcast data (water depth 11.5 m).

	T_p (s)												
H_s (m)	2	3	4	5	6	7	8	9	10	11	12	13	Σ
0.25	3.462	12.751	13.227	7.604	4.148	0.934	0.634	0.109	0.062	0.017	0.002		42.95
0.75		1.406	16.772	4.632	2.831	1.167	1.129	0.157	0.086	0.025	0.007	0.005	28.22
1.25			1.276	13.621	3.175	0.640	0.734	0.179	0.063	0.023	0.007	0.005	19.72
1.75				1.103	3.964	0.864	1.138	0.203	0.083	0.032	0.002		7.39
2.25					0.357	0.446	0.530	0.067	0.014	0.006	0.001		1.42
2.75					0.003	0.067	0.127	0.028	0.008	0.002	0.001		0.24
3.25						0.005	0.029	0.006	0.008	0.001			0.05
3.75							0.003	0.002	0.001	0.001			0.01
4.25							0.001	0.002					0.003
Σ	3.46	14.16	31.28	26.96	14.48	4.12	4.33	0.75	0.32	0.11	0.02	0.01	100.00

Note: $Pr(H_s, T_p)$ values in the table are given in percentage (%)

Table 3
Wave climate matrix for site S2 based on 35-years hindcast data (water depth 18.7 m).

	T_p (s)												
H_s (m)	2	3	4	5	6	7	8	9	10	11	12	13	Σ
0.25	0.768	4.225	8.363	6.844	3.930	1.018	0.515	0.034	0.013	0.005	0.002		25.72
0.75		1.055	10.619	9.852	7.153	2.399	2.709	0.376	0.074	0.014	0.002		34.25
1.25			0.665	9.289	7.404	1.556	1.744	0.592	0.351	0.082	0.001		21.68
1.75				0.476	7.218	1.335	1.093	0.268	0.284	0.124	0.011		10.81
2.25				0.006	1.065	2.253	0.936	0.158	0.109	0.076	0.023	0.003	4.63
2.75					0.044	0.405	1.189	0.098	0.057	0.045	0.022	0.005	1.86
3.25					0.002	0.016	0.534	0.085	0.030	0.018	0.012	0.012	0.71
3.75						0.001	0.117	0.085	0.030	0.009	0.004	0.002	0.25
4.25							0.007	0.039	0.015	0.007			0.07
4.75								0.005	0.004	0.006	0.001		0.02
5.25									0.002	0.001			0.003
5.75									0.001				0.001
Σ	0.77	5.28	19.65	26.47	26.82	8.98	8.84	1.74	0.97	0.39	0.08	0.02	100.00

Note: $Pr(H_s, T_p)$ values in the table are given in percentage (%)

in accordance with the parametric results of [19] obtained for the case of monochromatic waves. More specifically, according to that study, the placement of the aforementioned array close to the wall boundary induces hydrodynamic interactions between the WECs and the wall, that enhance the array's hydrodynamic behaviour and, thus, its power absorption ability, at periods larger than the heave natural period of the device. In the present investigation, the most frequent sea states for all examined sites (Tables 2–6) are characterized by T_p values larger than the WEC's heave natural period (equal to 2.6 s). The combination of the above advocates that maximization of E_{annual} can be achieved by placing the WECs close to the wall, as it has been verified from the optimum solution acquired in the case of OC1.

The annual averaged energy, E_{annual}, absorbed by the optimally-arranged WECs in the case of OC1 is shown in Fig. 6. The largest E_{annual} values among all sites, equal to 55.9 MWh and 55.3 MWh, are obtained for sites S4 and S5, respectively, whereas for sites S1~S3, situated in central Aegean (Cyclades), the annual energy absorption ability of the corresponding optimum layout configurations is reduced by 40.4%, 14.5%, 18.2%, respectively, compared to S4. In the case of site S3, the aforementioned reduction is attributed to the existence of milder local wave climate conditions (Table 4). However, this does not hold true for site S2, which has a local wave climate (Table 3) similar to that of S4 and S5. Nevertheless, in the case of S2, the WECs array is deployed at $h/a = 4$, contrary to sites S4~S5, where $h/a = 5$ has been taken into consideration. This reduces the finite depth spectral densities of the incident wave spectra at the former site, as shown in Fig. 7, where the TMA spectra for different h/a values are plotted indicatively for sea states with $H_s = 1.75$ m and $T_p = 4.0$ and 6.0 s. Accordingly, the optimally-arranged array realized in the case of S2 shows a smaller energy absorption ability. For site S1, the deployment of the WECs at an even smaller water depth (i.e., at $h/a = 3.5$) along with the existence of a milder local wave climate (Table 2) lead to the smallest E_{annual} value among all sites examined herein.

Regarding the second examined optimization case (OC2,

Table 4
Wave climate matrix for site S3 based on 35-years hindcast data (water depth 19.0 m).

	T_p (s)												
H_s (m)	2	3	4	5	6	7	8	9	10	11	12	13	Σ
0.25	4.645	14.973	13.044	4.479	2.839	0.912	1.185	0.176	0.050	0.016	0.005		42.32
0.75		1.710	13.182	9.510	1.547	0.393	0.624	0.173	0.085	0.033	0.006	0.004	27.27
1.25		0.001	0.290	10.038	6.446	0.255	0.190	0.043	0.038	0.016	0.014		17.33
1.75				0.148	8.237	0.656	0.193	0.015	0.013	0.003			9.27
2.25					0.644	1.968	0.275	0.011	0.005		0.001		2.90
2.75					0.002	0.154	0.528	0.009	0.005	0.001	0.001		0.70
3.25						0.001	0.166	0.007	0.002	0.001			0.18
3.75							0.023	0.002	0.001				0.026
4.25								0.001	0.001				0.002
Σ	4.65	16.68	26.52	24.17	19.72	4.34	3.18	0.44	0.20	0.07	0.03	0.01	100.00

Note: $Pr(H_s, T_p)$ values in the table are given in percentage (%)

Table 5
Wave climate matrix for site S4 based on 35-years hindcast data (water depth 19.2 m).

	T_p (s)												
H_s (m)	2	3	4	5	6	7	8	9	10	11	12	13	Σ
0.25	0.538	2.860	7.943	5.832	4.587	1.300	0.871	0.124	0.057	0.032	0.009	0.007	24.16
0.75		0.771	6.931	9.596	7.084	3.047	3.466	0.614	0.220	0.092	0.030	0.001	31.85
1.25			0.391	6.546	9.506	2.142	2.500	0.588	0.400	0.135	0.025	0.000	22.23
1.75			0.006	0.226	5.968	3.235	2.000	0.400	0.243	0.166	0.048	0.001	12.29
2.25					0.374	2.034	2.789	0.159	0.132	0.085	0.053	0.022	5.65
2.75					0.002	0.084	1.968	0.135	0.033	0.031	0.015	0.006	2.27
3.25						0.001	0.572	0.301	0.024	0.009	0.004	0.001	0.91
3.75							0.027	0.339	0.036	0.004			0.41
4.25								0.051	0.102	0.002			0.16
4.75									0.038	0.005			0.04
5.25									0.009	0.014			0.02
5.75										0.002			0.002
Σ	0.54	3.63	15.27	22.20	27.52	11.84	14.19	2.71	1.29	0.58	0.18	0.04	100.00

Note: $Pr(H_s, T_p)$ values in the table are given in percentage (%)

Table 1), where the linear array is fixed at $c/a = 1.1$, as resulted from OC1, and the WECs are enabled to be distributed along a part of the available wall length (i.e., at $10 \leq X/a \leq 26$), the corresponding optimum results are presented in Fig. 8. For all examined sites, optimum layout configurations are realized by placing the middle WEC (WEC3) close to $X/a \approx 18$ (middle of the wall) and the two outer WECs (WEC1 and WEC5) at the two edges of the available wall length (i.e., at $X_1/a = 10$ and $X_5/a = 26$ respectively, as resulted from Eq. (3a)). For sites S3 and S4, the positioning of the rest of the devices (WEC2 and WEC4) along the *OX* axis leads to the formation of an array with almost equally-spaced devices. For sites S1, S2 and S5, WEC4 is situated a bit more closely to the corresponding outer device (i.e., WEC5).

As for the maximized values of E_{annual} obtained in the case of OC2 (Fig. 9), the optimally-arranged WECs located at sites S4 and S5 absorb again the largest amounts of annual energy equal to 55.8 MWh and 55.2 MWh, respectively. For sites S1~S3, the energy absorption ability of the optimized linear array is reduced, respectively, by 40.8%, 14.6% and 18.2%, compared to S4. The above results are very similar with those obtained for OC1 and, hence, the relevant discussion made above can be utilized for their physical interpretation.

The optimization results related to the final examined optimization case (OC3, Table 1) are presented in Figs. 10 and 11. It is recalled that for OC3 the linear array is again fixed at $c/a = 1.1$, as in OC2; however, the two outer WECs are allowed to be situated within l_{out}, facilitating the formation of optimum array layouts within the total available wall length (i.e., at $0 \leq X/a \leq 36$). As shown in Fig. 10, for all sites examined and contrary to OC1 and OC2, the optimum solutions correspond to a random placement of the WECs in front of the wall boundary, with unequal center-to-center distances between adjacent devices. The most distinctive feature of the optimally-arranged arrays is the formation of two clusters of closely-positioned WECs. Each cluster consists of either three or two devices and it is situated close to one of the two wall edges. As for the annual energy absorbed by the linear array (Fig. 11), the

Table 6
Wave climate matrix for site S5 based on 35-years hindcast data (water depth 27.0 m).

	T_p (s)												
H_s (m)	2	3	4	5	6	7	8	9	10	11	12	13	Σ
0.25	0.443	2.810	7.965	6.088	3.380	0.796	0.528	0.046	0.021	0.010	0.002	0.001	22.09
0.75		0.586	7.112	11.264	8.646	2.487	2.106	0.252	0.093	0.017	0.001		32.56
1.25			0.395	6.299	11.037	3.351	2.199	0.264	0.166	0.040	0.003		23.75
1.75				0.243	5.209	4.105	2.996	0.197	0.087	0.038	0.009		12.88
2.25					0.418	1.417	3.686	0.298	0.077	0.016	0.010		5.92
2.75					0.010	0.147	1.179	0.538	0.081	0.018	0.003		1.98
3.25						0.010	0.205	0.251	0.135	0.005	0.002		0.61
3.75							0.047	0.042	0.057	0.020			0.17
4.25							0.008	0.017	0.005	0.002	0.001		0.03
4.75								0.005		0.001			0.01
5.25										0.001	0.001		0.002
Σ	0.44	3.40	15.47	23.89	28.70	12.31	12.95	1.91	0.72	0.17	0.03	0.001	100.00

Note: $Pr(H_s, T_p)$ values in the table are given in percentage (%)

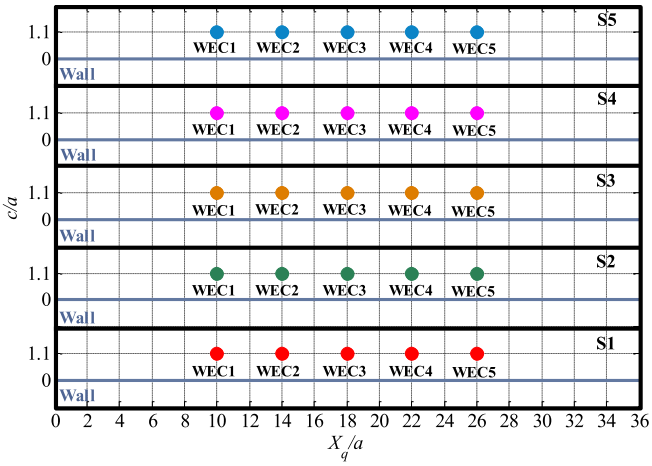

Fig. 5. Optimum layout configurations of the WECs array in front of the wall for S1~S5 and for OC1.

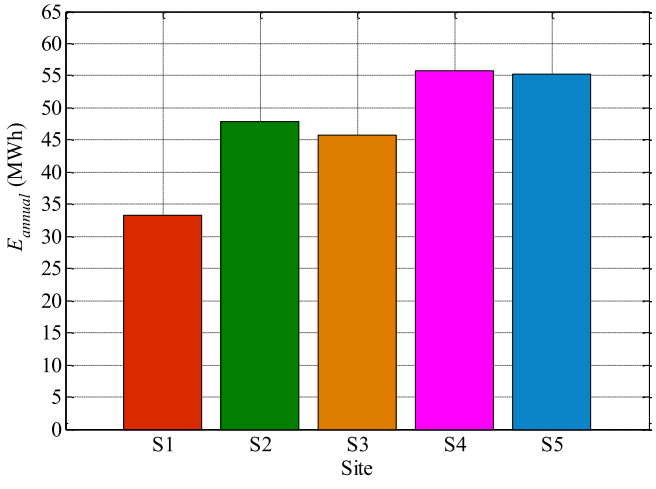

Fig. 6. E_{annual} absorbed by the optimally-arranged WECs arrays at S1~S5 for OC1.

largest E_{annual} values equal to 60.8 MWh and 60.5 MWh are obtained for the optimally-arranged arrays located at sites S4 and S5, respectively, as in the case of OC1 (Fig. 6) and OC2 (Fig. 9). Compared to S4, the corresponding E_{annual} for the rest examined sites is reduced by 37.3% (site S1), 11.1% (site S2) and 14.9% (site S3) for the reasons previously explained.

In order to demonstrate the effect of the different optimally-arranged WEC arrays on E_{annual}, a comparison of the latter quantity among OC1~OC3 for all examined sites is made. The corresponding results are shown in Fig. 12. For a given marine site, the consideration of a part of the available wall length for placing the WECs (OC2) does not introduce any substantial difference on E_{annual} compared to OC1. This is attributed to fact that the optimum solutions of OC2 correspond to arrays with almost equally-spaced devices (Fig. 8), resembling the arrays of OC1, where the WECs had a predefined uniform distribution along *OX*. However, when the two outer WECs of the array are enabled to be situated within a length close to the wall edges, facilitating the utilization of the total available wall length for placing the devices and, thus, the realization of a wider distribution of the WECs along the leeward boundary (OC3), the annual energy absorption ability of the optimally-arranged arrays is improved for all examined sites. More specifically, E_{annual} is increased by 14.3% (site S1), 13.2% (site S2), 13.1% (site S3), 8.9% (site S4) and 9.4% (site S5), compared to OC1 while the corresponding percentages relevant to OC2 are 15.5%, 13.6%, 13.4%, 9.1% and 9.6% for sites S1~S5 respectively.

Finally, it is interesting to illustrate the contribution of each WEC (%) to the maximized E_{annual}. This is realized with the aid of Fig. 13. In the case of OC1 (Fig. 13a) and OC2 (Fig. 13b) and for sites S2~S5, the two outer WECs (WEC1 and WEC5) contribute a bit more to the total annual energy absorbed by the optimum array layouts compared to the rest of the WECs. A different trend is observed for site S1, where a bit larger contribution is observed for WEC3 (middle WEC). For this site, the finite depth spectral densities of the sea states with $T_p = 6.0$ s are greatly reduced due to the consideration of $h/a = 3.5$ s (Fig. 7b). Accordingly, and contrary to S2~S5, the optimized array absorbs a significant amount of energy only for sea states with 4.0 s$\leq T_p \leq$5.0 s. In this period range, WEC3 shows a larger heave response compared to the rest WECs (results are not included here due to space constraints), and, thus, it contributes more to E_{annual}. Regarding OC3 (Fig. 13c), the outer WEC of the 2-

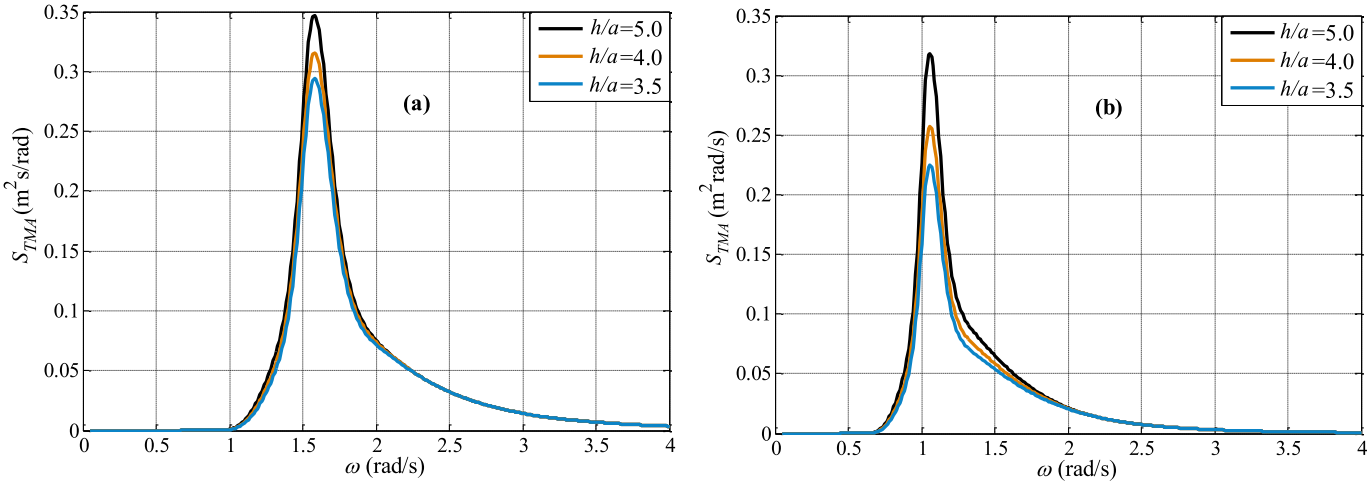

Fig. 7. Effect of h/a on S_{TMA} for sea states with H_s = 1.75 m and T_p = 4.0 s **(a)** and 6.0 s **(b)**.

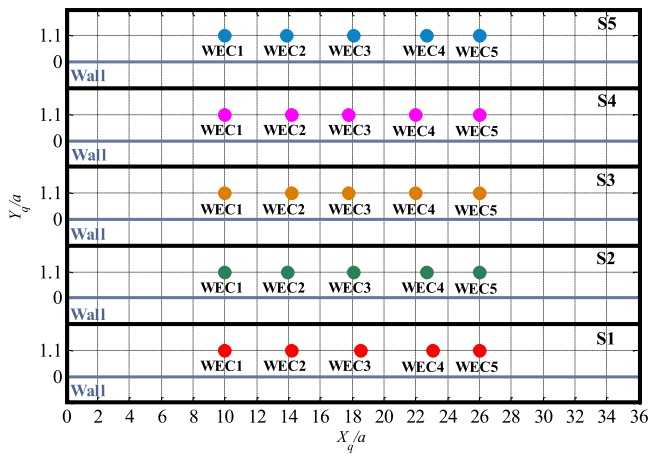

Fig. 8. Optimum layout configurations of the WECs array in front of the wall for S1~S5 and for OC2.

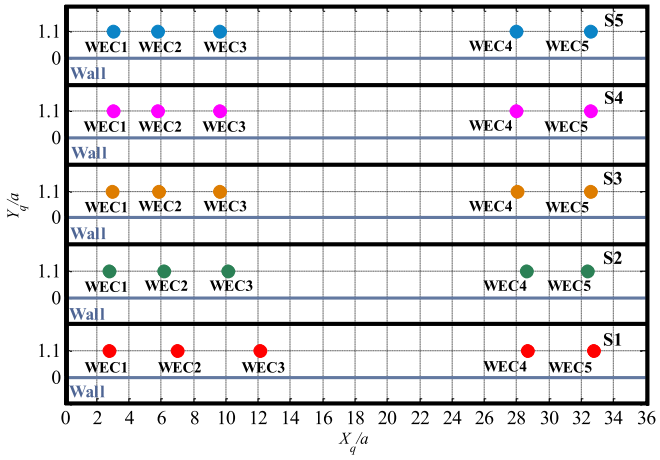

Fig. 10. Optimum layout configurations of the WECs array in front of the wall for S1~S5 and for OC3.

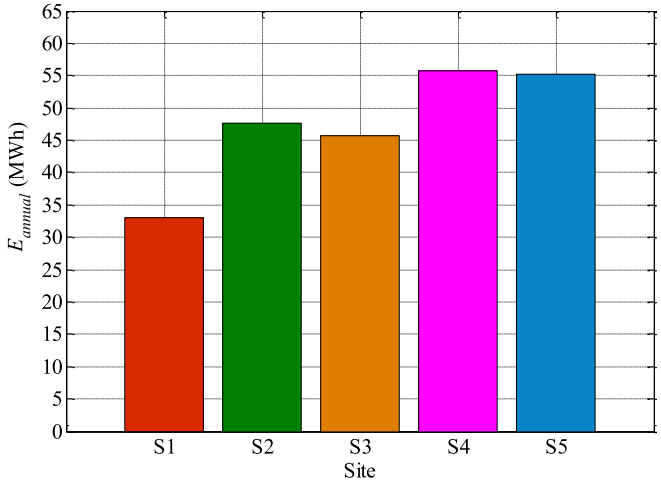

Fig. 9. E_{annual} absorbed by the optimally-arranged WECs arrays at S1~S5 for OC2.

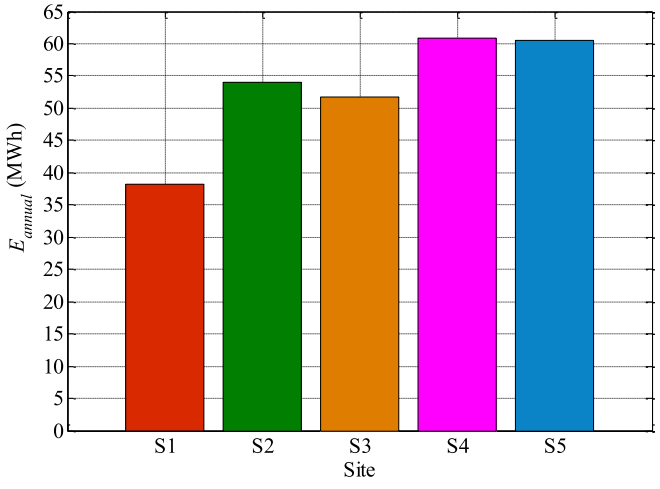

Fig. 11. E_{annual} absorbed by the optimally-arranged WECs arrays at S1~S5 for OC3.

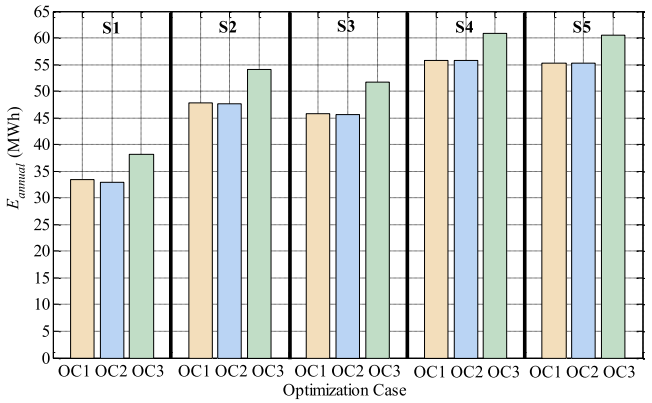

Fig. 12. Effect of different optimum array layouts on E_{annual} for each examined site.

body cluster (i.e., WEC5, see Fig. 10) for all sites examined contributes a bit more to the maximized E_{annual}, followed by either WEC4 (inner WEC of the 2-body cluster, Fig. 10) in the case of S4~S5 or WEC2 (middle WEC of the 3-body cluster, Fig. 10) for sites S2~S3 or, finally, WEC1 (outer WEC of the 3-body cluster, Fig. 10) in the case of S1. It should be noted, however, that for all optimization cases and sites considered herein, the WECs' contributions to E_{annual} differ slightly among the various WECs of each optimally-arranged array and the corresponding percentages have values very close to 20%. This, in turn, demonstrates an almost equal contribution of the 5 WEC units of the optimally-arranged arrays to the annual absorbed energy.

6. Conclusions

In the present paper, we developed an optimization numerical framework to determine the optimum layout of a linear array of oblate spheroidal heaving WECs in front of a vertical, bottom-mounted wall of finite length under the action of perpendicular to the arrangement long-crested irregular waves. The term "optimum" corresponds to layouts that maximize the annual averaged energy absorbed by the array, while satisfying specific spatial constraints. The developed framework is applied for an array of five WECs deployed at five near-shore sites in the Aegean Sea, Greece, which are characterized by mild wave conditions. For each site, three different optimization cases are solved (OC1~OC3), facilitating the investigation of various aspects of the examined physical problem. The main conclusions of this study for the WECs'

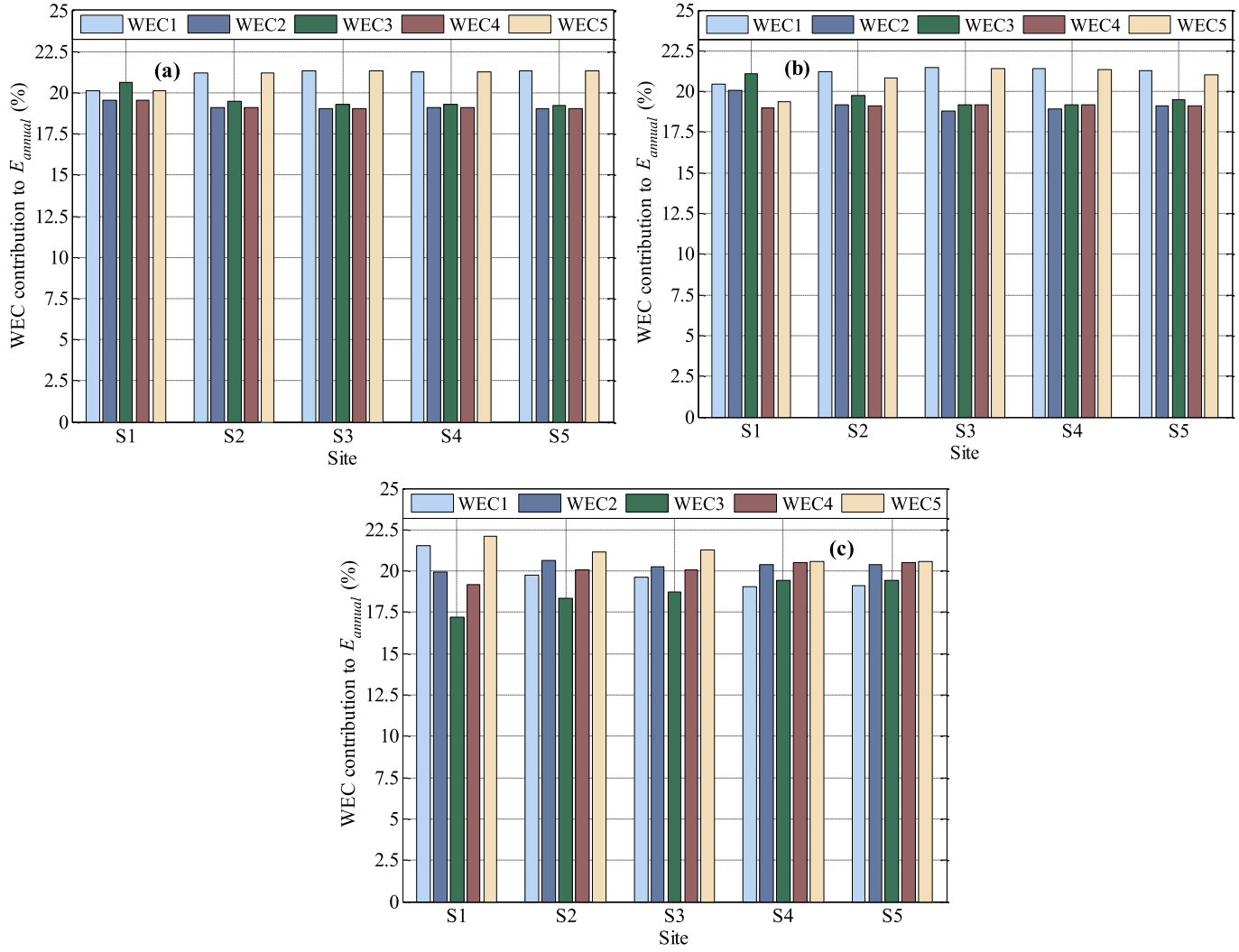

Fig. 13. Contribution of each WEC of the optimally-arranged arrays on E_{annual} for S1~S5 and for OC1 **(a)**, OC2 **(b)** and OC3 **(c)**.

geometrical/operational characteristics and wave climate conditions considered can be summarized as follows:

- For the linear array consisting of equally-spaced WECs at predefined, fixed, positions along a part of the available wall length (OC1), optimally-arranged layouts for all sites are realized by placing the array at the smallest allowable non-dimensional perpendicular distance from the wall boundary (i.e., at $c/a = 1.1$). From a physical point, this could be related to the deployment of WECs with heave natural period smaller than the peak periods of the most frequent sea states. When the linear array is assumed fixed at $c/a = 1.1$, while the devices are free to be situated along a part of the available wall length (OC2), optimum layouts consist of almost equally-spaced devices, resembling the array configurations of OC1. However, when the two outer WECs are allowed to be situated along a length close to the wall edges, facilitating the distribution of the devices within the total available wall length (OC3), optimum layouts are characterized by the formation of two clusters of either two or three closely-positioned WECs, situated close to each wall edge.
- For all optimization cases examined, the largest values of the annual energy, E_{annual}, absorbed by the optimally-arranged arrays are obtained for sites S4 and S5 in south-eastern Aegean, with the arrays deployed at S5 showing a slightly reduced (by an average of 0.8%) annual absorption ability. Compared to S4, E_{annual} is reduced by an average of 17.1% in the case of site S3 (central Aegean), due the existence of a milder local wave environment. For site S2 (central Aegean), a reduction of the finite depth spectral densities of the incident wave spectra occurs, since the WECs array is deployed at a smaller water depth. Thus, for this site, an average reduction of E_{annual} by 13.4% compared to S4 is realized. Regarding site S1 (central Aegean), the existence of an even smaller water depth combined with milder local wave conditions lead to a significant, equal to 39.5%, average reduction of the energy absorption ability of the corresponding optimally-arranged clusters compared to S4.
- By allowing the outer WECs of the array to be situated within a length close to the wall edges and, thus, enabling the utilization of the whole available wall length for placing the devices, the energy absorption ability of the linear array is enhanced. Specifically, E_{annual} is increased by an average (among all sites) 12.2% and 11.8% compared, respectively, to OC2 (free placement of WECs along a part of the total wall length) and OC1 (fixed, with an equal spacing, placement of WECs along a part of the total wall length).
- For all optimization cases and sites examined herein, the five WEC units of the optimally-arranged arrays show an almost equal contribution to the maximized annual absorbed energy.

The developed optimization framework is generic and can be easily applied to various layout optimization problems of heaving WECs arrays in front of a wall, by appropriately modifying the spatial constraints. Accordingly, optimum array layouts could be determined for the case, where the WECs are allowed to be situated at different perpendicular distances from the wall. The determination of optimally-arranged arrays consisting of WECs with heave natural period closer to the peak periods of the most frequent sea states, the effect of the wave directionality on the optimum layouts' formation and the annual absorbed energy, as well as the inclusion of cost-related aspects in the formation of the optimization problem could also present items for future investigation.

CRediT authorship contribution statement

Eva Loukogeorgaki: Conceptualization, Methodology, Investigation, Software, Formal analysis, Data curation, Writing – original draft, Writing – review & editing. **Constantine Michailides:** Conceptualization, Methodology, Investigation, Software, Formal analysis, Data curation, Writing – original draft, Writing – review & editing. **George Lavidas:** Conceptualization, Methodology, Investigation, Software, Formal analysis, Data curation, Writing – original draft, Writing – review & editing. **Ioannis K. Chatjigeorgiou:** Conceptualization, Writing – review & editing.

Declaration of competing interest

The authors declare that they have no known competing financial interests or personal relationships that could have appeared to influence the work reported in this paper.

References

[1] COM, Communication from the Commission to the European Parliament, the Council, the European Economic and Social Committee and the Committee of the Regions: an EU Strategy to Harness the Potential of Offshore Renewable Energy for a Climate Neutral Future, European Commission, Brussels, 2020. Available online, https://eur-lex.europa.eu/legal-content/EN/TXT/?uri=COM%3A2020%3A741%3AFIN&qid=1605792629666 (accessed on 5 March 2021).
[2] E. Rusu, F. Onea, A review of the technologies for wave energy extraction, Clean Energy 2 (1) (2018) 10–19, https://doi.org/10.1093/ce/zky003.
[3] D. Qiao, R. Haider, J. Yan, D. Ning, B. Li, Review of wave energy converter and design of mooring system, Sustainability 12 (19) (2020) 8251, https://doi.org/10.3390/su12198251.
[4] D. Magagna, R. Monfardini A, Uihlein JRC Ocean Energy Status Report: 2016 Edition, EUR 28407 EN (JRC104799), Publications Office of the European Union, Luxembourg, 2016, pp. 10–13.
[5] V. Stratigaki, P. Troch, T. Stallard, D. Forehand, J.P. Kofoed, M. Folley, M. Benoit, A. Babarit, J. Kirkegaard, Wave basin experiments with large wave energy converter arrays to study interactions between the converters and effects on other users in the sea and the coastal area, Energies 7 (2) (2014) 701–734, https://doi.org/10.3390/en7020701.
[6] M. Penalba, I. Touzón, J. Lopez-Mendia, V. Nava, A numerical study on the hydrodynamic impact of device slenderness and array size in wave energy farms in realistic wave climates, Ocean Eng. 142 (2017) 224–232, https://doi.org/10.1016/j.oceaneng.2017.06.047.
[7] P. Balitsky, G.V. Fernandez, V. Stratigaki, P. Troch, Assessment of the power output of a two-array clustered WEC farm using a BEM solver coupling and a wave-propagation model, Energies 11 (11) (2018) 2907, https://doi.org/10.3390/en11112907.
[8] G. Lavidas, Selection index for Wave Energy Deployments (SIWED): a near-deterministic index for wave energy converters, Energy 196 (2020) 117131, https://doi.org/10.1016/j.energy.2020.117131.
[9] M.A. Mustapa, O.B. Yaakob, Y.M. Ahmed, C.-K. Rheem, K.K. Koh, F.A. Adnan, Wave energy device and breakwater integration: a review, Renew. Sustain. Energy Rev. 77 (2017) 43–58, https://doi.org/10.1016/j.rser.2017.03.110.
[10] X.L. Zhao, D.Z. Ning, Q.P. Zou, D.S. Qiao, S.Q. Cai, Hybrid floating breakwater-WEC system: a review, Ocean Eng. 186 (2019) 106126, https://doi.org/10.1016/j.oceaneng.2019.106126.
[11] P. Rosa-Santos, F. Taveira-Pinto, D. Clemente, T. Cabral, F. Fiorentin, F. Belga, T. Morais, Experimental study of a hybrid wave energy converter integrated in a harbor breakwater, J. Mar. Sci. Eng. 7 (2) (2019) 33, https://doi.org/10.3390/jmse7020033.
[12] V T. Calheiros-Cabral, D. Clemente, P. Rosa-Santos, F. Taveira-Pinto, V. Ramos, T. Morais, H. Cestaro, Evaluation of the annual electricity production of a hybrid breakwater integrated wave energy converter, Energy 213 (2020) 118845, https://doi.org/10.1016/j.energy.2020.118845.
[13] D. Vicinanza, L. Margheritini, J.P. Kofoed, M. Buccino, The SSG wave energy converter: performance, status and recent developments, Energies 5 (2) (2012) 193–226, https://doi.org/10.3390/en5020193.
[14] C. Michailides, C.D.C. Angelides, Optimization of a flexible floating structure for wave energy production and protection effectiveness, Eng. Struct. 85 (2015) 249–263, https://doi.org/10.1016/j.engstruct.2014.12.031.
[15] S.A. Mavrakos, G.M. Katsaounis, K. Nielsen, G. Lemonis, Numerical performance investigation of an array of heaving wave power converters in front of a vertical breakwater, Proc. 14th Int. Offshore Polar Eng. Conf., Toulon, France (3) (2004) 1170–1178. May 23–28.
[16] D.N. Konispoliatis, S.A. Mavrakos, Wave power absorption by arrays of wave energy converters in front of a vertical breakwater: a theoretical study, Energies 13 (8) (2020) 1985, https://doi.org/10.3390/en13081985.
[17] D.N. Konispoliatis, S.A. Mavrakos, G.M. Katsaounis, Theoretical evaluation of

the hydrodynamic characteristics of arrays of vertical axisymmetric floaters of arbitrary shape in front of a vertical breakwater, J. Mar. Sci. Eng. 8 (1) (2020) 62, https://doi.org/10.3390/jmse8010062.
[18] E. Loukogeorgaki, I.K. Chatjigeorgiou, Hydrodynamic performance of an array of wave energy converters in front of a vertical wall, in: Proceedings 13th European Wave and Tidal Energy Conference, Napoli, Italy, 2019, p. 1464. September 1–6, 2019.
[19] E. Loukogeorgaki, I. Boufidi, I.K. Chatjigeorgiou, Performance of an array of oblate spheroidal heaving wave energy converters in front of a wall, Water 12 (1) (2020) 188, https://doi.org/10.3390/w12010188.
[20] M. Göteman, M. Giassi, J. Engström, J. Isberg, Advances and challenges in wave energy park optimization – a review, Front. Energy Res. 8 (2020), https://doi.org/10.3389/fenrg.2020.00026.
[21] B.F.M. Child, V. Venugopal, Optimal configurations of wave energy device arrays, Ocean Eng. 37 (16) (2010) 1402–1417, https://doi.org/10.1016/j.oceaneng.2010.06.010.
[22] C. Sharp, B. DuPont, Wave energy converter array optimization: a genetic algorithm approach and minimum separation distance study, Ocean Eng. 163 (2018) 148–156, https://doi.org/10.1016/j.oceaneng.2018.05.071.
[23] P.M. Ruiz, V. Nava, M.B.R. Topper, P.R. Minguela, F. Ferri, J.P. Kofoed, Layout optimisation of wave energy converter arrays, Energies 10 (9) (2017) 1262, https://doi.org/10.3390/en10091262.
[24] D. Sarkar, E. Contal, N. Vayatis, F. Dias, Prediction and optimization of wave energy converter arrays using a machine learning approach, Renew. Energy 97 (2016) 504–517, https://doi.org/10.1016/j.renene.2016.05.083.
[25] M. Neshat, E. Abbasnejad, Q. Shi, B. Alexander, M. Wagner, Adaptive neuro-surrogate-based optimisation method for wave energy converters placement optimisation, in: Proceedings 26th International Conference on Neural Information Processing, Sydney, Australia, 2019, pp. 353–366, https://doi.org/10.1007/978-3-030-36711-4_30. December 12–15.
[26] C.H. Lee, WAMIT Theory Manual, 1995. Available online: https://www.wamit.com/Publications/tmanual.pdf. (Accessed 5 March 2021).
[27] C.H. Lee, J.N. Newman, Computation of wave effects using the panel method, in: S. Chakrabarti (Ed.), Numerical Models in Fluid-Structure Interaction, WIT Press, Southampton, UK, 2005, pp. 211–251.
[28] S.A. Kitaigordskii, V.P. Krasitsikii, M.M. Zaslavskii, On Phillips' theory of equilibrium range in the spectra of wind-generated gravity waves, J. Phys. Oceanogr. 5 (1975) 410–420, https://doi.org/10.1175/1520-0485(1975)005<0410:OPTOER>2.0.CO;2.
[29] S.A. Hughes, The TMA Shallow-Water Spectrum Description and Applications, Technical Report CERC-84-7, Coastal Engineering Research Center, Department of the Army, US Army Corps of Engineers, 1984.
[30] E. Bouws, H. Gunter, W. Rosenthal, C.L. Vincent, Similarity of the wind wave spectrum in finite water depth: 1. Spectral form, J. Geophys. Res. 90 (1985) 975–986, https://doi.org/10.1029/JC090iC01p00975.
[31] L. Bergdahl, Comparison of measured shallow-water wave spectra with theoretical spectra, in: Proceedings of the 8th European Wave and Tidal Energy Conference, Uppsala, Sweden, 2009. September 7–10.
[32] Det Norske Veritas–Germanischer Lloyds (DNV–GL), Environmental Conditions and Environmental Loads, Recommended Practice, 2017. DNVGL-RP-C205, DNV-GL, Oslo, Norway.
[33] MATLAB and Optimization Toolbox R2019b, The MathWorks, Inc., Natick, Massachusetts, United States.
[34] MATLAB R2019b, The MathWorks, Inc., Natick, Massachusetts, United States.
[35] J. Salmon, L. Holthuijsen, P. Smit, G.P. van Vledder, M. Zijlema, Alternative source terms for SWAN in the coastal region, in: Proceedings of the 34th International Conference on Coastal Engineering, Seoul, Korea, 2014, p. 14. June 15–20.
[36] G.P. van Vledder, M. Zijlema, L.H. Holthuijsen, Revisiting the JONSWAP bottom friction formulation, in: Proceedings of 32nd Conference on Coastal Engineering, Shanghai, China, 2010, p. 8, https://doi.org/10.9753/icce.v32.waves.41. June 30–July 5.
[37] M. Zijlema, G.P. van Vledder, L.H. Holthuijsen, Bottom friction and wind drag for wave models, Coast. Eng. 65 (2012) 19–26, https://doi.org/10.1016/j.coastaleng.2012.03.002.
[38] L. Cavaleri, F. Barbariol, A. Benetazzo, Wind–wave modeling: where we are, where to go, J. Mar. Sci. Eng. 8 (4) (2020) 260, https://doi.org/10.3390/jmse8040260.
[39] B. Kamranzad, N. Mori, Future wind and wave climate projections in the Indian Ocean based on a super-high-resolution MRI-AGCM3.2S model projection, Clim. Dynam. 53 (2019) 2391–2410, https://doi.org/10.1007/s00382-019-04861-7.
[40] G. Lavidas, V. Venugopal, D. Friedrich, Sensitivity of a numerical wave model on wind re-analysis datasets, Dynam. Atmos. Oceans 77 (2017) 1–16, https://doi.org/10.1016/j.dynatmoce.2016.10.007.
[41] J.E. Stopa, Wind forcing calibration and wave hindcast comparison using multiple reanalysis and merged satellite wind datasets, Ocean Model. 127 (2018) 55–69, https://doi.org/10.1016/J.OCEMOD.2018.04.008.
[42] G.P. van Vledder, A. Akpinar, Wave model predictions in the Black Sea: sensitivity to wind fields, Appl. Ocean Res. 53 (2015) 161–178, https://doi.org/10.1016/j.apor.2015.08.006.
[43] G. Lavidas, H. Polinder, North Sea Wave Database (NSWD) and the need for reliable resource data: a 38 year database for metocean and wave energy assessments, Atmosphere 10 (9) (2019) 551, https://doi.org/10.3390/atmos10090551.
[44] G. Lavidas, V. Venugopal, A 35 year high-resolution wave atlas for nearshore energy production and economics at the Aegean Sea, Renew. Energy 103 (2017) 401–417, https://doi.org/10.1016/j.renene.2016.11.055.
[45] G. Lavidas, A. Agarwal, V. Venugopal, Availability and accessibility for offshore operations in the Mediterranean Sea, J. Waterw. Port, Coast. Ocean Eng. 144 (6) (2018), 05018006, https://doi.org/10.1061/(ASCE)WW.1943-5460.0000467.
[46] I.K. N. Tzellos, E. Loukogeorgaki, E. Anastasiou, I.K. Chatjigeorgiou, Performance of an oblate spheroidal heaving wave energy converter, in: Proceedings of the 30th International Offshore and Polar Engineering Conference, Shanghai, China vol. 1, 2020, pp. 116–123. October 11-16
[47] J. Falnes, A. Kurniawan, Ocean Waves and Oscillating Systems: Linear Interactions Including Wave-Energy Extraction, second ed., Cambridge University Press, Cambridge, UK, 2020, pp. 20–23.
[48] S. Saha, S. Moorthi, H. Pan, X. Wu, J. Wang, S. Nadiga, et al., The NCEP climate forecast system reanalysis, Bull. Am. Meteorol. Soc. 91 (8) (2010) 1015–1058, https://doi.org/10.1175/2010BAMS3001.1.